

Experimental measurement for the expectation value of the product of two noncommuting observables via weak measurement in a trapped-ion system

Wenbo Su, Manchao Zhang, Chunwang Wu[✉], Yi Xie, Han Hu, Ting Chen, Tianxiang Zhan[✉], Baoquan Ou, Wei Wu, Jie Zhang^{✉,*} and Pingxing Chen[†]

*Institute for Quantum Science and Technology, College of Science,
National University of Defense Technology, Changsha 410073, Hunan, China;
Hefei National Laboratory, Hefei 230088, China;*

and Hunan Key Laboratory of Mechanism and Technology of Quantum Information, Changsha 410073, Hunan, China

 (Received 16 March 2023; revised 14 June 2023; accepted 11 September 2023; published 2 October 2023)

The expectation value of the product of two noncommuting observables (POTNO) can be used to test the commutation relation and dig out the correlation between two observables. However, since a POTNO is generally a non-Hermitian operator, its average cannot be measured directly according to standard quantum mechanics. Recently, a theoretical scheme has been proposed to obtain POTNOs, but the observables are limited to projection operators. In this paper, we present a scheme that employs weak measurement to directly measure the expectation value of the POTNO, where the observables are arbitrary operators. Our scheme transforms the measurement of this expectation value into the measurements of several single observable weak values. Experimentally we demonstrate our scheme by measuring the expectation value of the product of two Pauli operators and verify their commutation and anticommutation relations in a trapped-ion system. Moreover, our scheme is applicable to the cases with more than two observables.

DOI: [10.1103/PhysRevA.108.042601](https://doi.org/10.1103/PhysRevA.108.042601)

I. INTRODUCTION

Compared with classical physics, quantum physics has many mysterious phenomena. One of the important phenomena is that we cannot accurately measure the information of two arbitrary noncommuting observables \hat{A} and \hat{B} simultaneously [1,2]. This progress can be described mathematically as $\Delta\hat{A}\Delta\hat{B} \geq \frac{1}{2}|\langle[\hat{A}, \hat{B}]\rangle|$. In the last two decades, some uncertainty relations have been verified by measuring the value of $\Delta\hat{A}\Delta\hat{B}$ [3–7] and some commutation relations were demonstrated in different experimental systems [8–12]. However, direct measurement of the expectation value of the product of two variables, $\langle\hat{A}\hat{B}\rangle$, which is known as the correlation function in statistical mechanics and used for analyzing their correlations [13,14], is quite elusive due to fact that the product of two arbitrary noncommuting observables is non-Hermitian. In quantum projective measurement, quantum-mechanical observables are limited to Hermitian operators [15], while non-Hermitian operators commonly exist in open physical systems, such as a broken parity-time symmetric Hamiltonian [16–18]. The average of a non-Hermitian operator is usually a complex number, which is beyond the scope of projective measurement [19,20].

To measure the expectation value of a product of two noncommuting observables (POTNO), the weak measurement proposed by Aharonov *et al.* [21] is a suitable tool [22–26]. In 2015, Pati *et al.* proposed a theoretical scheme to measure the expectation value of any non-Hermitian operator via weak

measurement [27]. However, in their scheme, only the average of the product of two special operators, i.e., projection operators, is measured. Recently, Wagner *et al.* presented a work that directly measures the expectation value of commutation relation for Pauli operators by using weak measurement [28]. They ingeniously transform the expectation value of the commutation relation for Pauli operators into the product of a single weak value of projector and the probability of postselection. In this case, the dilemma of direct measurement of the expectation value of the product of Pauli operators is avoided.

In this paper, we present a direct scheme to measure the expectation value of the product of two arbitrary qubit operators. Our scheme inserts identity operator into the expectation value of the product of two arbitrary adjacent qubit observables. Then this expectation value can be calculated by multiplying the single observable weak values and the projective probability. This scheme is further verified by measuring the average of the product of Pauli operators with a single trapped ion. Lastly, the measured values are used to verify the commutation and anticommutation relation between Pauli operators.

II. THEORETICAL MODEL

In this section, our scheme for measuring the expectation value of the POTNOs \hat{A} and \hat{B} in a two-level system is introduced.

To begin with, let us review the principle of weak measurement. The concept of weak measurement is introduced on the basis of the von Neumann measurement model [29]. The Hamiltonian of the measured system and the measuring pointer can be written as

$$H_I = g\hat{A} \otimes \hat{p}, \quad (1)$$

*zj1589233@126.com

†pxchen@nudt.edu.cn

where g is the coupling strength between measured system and measuring pointer, \hat{A} is the observable of measured system, and \hat{p} is the canonical momentum of measuring pointer. In weak measurement, the coupling strength g is so small that the measured system is not completely ‘‘collapsed’’. If the measured system’s initial state is selected to be $|\psi\rangle$ and the postselection state is $|\psi_f\rangle$, the displacement of the measuring pointer can be measured as $g\langle\hat{A}\rangle_w^{\psi_f,\psi}$, where $\langle\hat{A}\rangle_w^{\psi_f,\psi}$ is a weak value defined as

$$\langle\hat{A}\rangle_w^{\psi_f,\psi} = \frac{\langle\psi_f|\hat{A}|\psi\rangle}{\langle\psi_f|\psi\rangle}. \quad (2)$$

From the definition of the weak value $\langle\hat{A}\rangle_w^{\psi_f,\psi}$, the weak value can beyond the eigenvalue spectrum of the observable \hat{A} . In particular, the complex results for weak values can be applied to quantum measurement [30].

The following shows the use of weak measurement to measure the expectation value of $\hat{A}\hat{B}$ in our scheme. At first, we need to select a complete set for the measurement basis, for example $|\uparrow\rangle$ and $|\downarrow\rangle$ (the eigenstates of the Pauli operator $\hat{\sigma}_z$). Then this basis is inserted into the formula $\langle\hat{A}\hat{B}\rangle$. If the measured initial state is $|\psi\rangle$, the expectation value of the operator $\hat{A}\hat{B}$ in a two level system is written as

$$\begin{aligned} \langle\psi|\hat{A}\hat{B}|\psi\rangle &= \langle\psi|\hat{A}|\uparrow\rangle\langle\uparrow|\hat{B}|\psi\rangle + \langle\psi|\hat{A}|\downarrow\rangle\langle\downarrow|\hat{B}|\psi\rangle \\ &= |\langle\uparrow|\psi\rangle|^2 \frac{\langle\psi|\hat{A}|\uparrow\rangle}{\langle\psi|\uparrow\rangle} \frac{\langle\uparrow|\hat{B}|\psi\rangle}{\langle\uparrow|\psi\rangle} + |\langle\downarrow|\psi\rangle|^2 \\ &\quad \times \frac{\langle\psi|\hat{A}|\downarrow\rangle}{\langle\psi|\downarrow\rangle} \frac{\langle\downarrow|\hat{B}|\psi\rangle}{\langle\downarrow|\psi\rangle} \\ &= |\langle\uparrow|\psi\rangle|^2 \langle\hat{A}\rangle_w^{\psi,\uparrow*} \langle\hat{B}\rangle_w^{\psi,\uparrow} + |\langle\downarrow|\psi\rangle|^2 \langle\hat{A}\rangle_w^{\psi,\downarrow*} \langle\hat{B}\rangle_w^{\psi,\downarrow}, \end{aligned} \quad (3)$$

where $|\langle\uparrow|\psi\rangle|^2$ is the probability of the initial state $|\psi\rangle$ projected to final state $|\uparrow\rangle$, $\langle\hat{A}\rangle_w^{\psi,\uparrow}$ is the weak value of the operator \hat{A} for a postselected state $|\uparrow\rangle$ and preselected state $|\psi\rangle$, and $\langle\hat{A}\rangle_w^{\psi,\uparrow*}$ is the conjugate number of $\langle\hat{A}\rangle_w^{\psi,\uparrow}$.

To verify the accuracy of our scheme, the expectation value of the commutation relation for observables \hat{A} and \hat{B} can be measured using Eq. (3). The expectation value of their commutation relation can be rewritten as

$$\begin{aligned} \langle\psi|[\hat{A}, \hat{B}]|\psi\rangle &= \langle\psi|\hat{A}\hat{B}|\psi\rangle - \langle\psi|\hat{B}\hat{A}|\psi\rangle \\ &= (|\langle\uparrow|\psi\rangle|^2 \langle\hat{A}\rangle_w^{\psi,\uparrow*} \langle\hat{B}\rangle_w^{\psi,\uparrow} + |\langle\downarrow|\psi\rangle|^2 \\ &\quad \times \langle\hat{A}\rangle_w^{\psi,\downarrow*} \langle\hat{B}\rangle_w^{\psi,\downarrow}) \\ &\quad - (|\langle\uparrow|\psi\rangle|^2 \langle\hat{B}\rangle_w^{\psi,\uparrow*} \langle\hat{A}\rangle_w^{\psi,\uparrow} \\ &\quad + |\langle\downarrow|\psi\rangle|^2 \langle\hat{B}\rangle_w^{\psi,\downarrow*} \langle\hat{A}\rangle_w^{\psi,\downarrow}), \end{aligned} \quad (4)$$

and the anticommutation relation can be rewritten as

$$\begin{aligned} \langle\psi|\{\hat{A}, \hat{B}\}|\psi\rangle &= |\langle\uparrow|\psi\rangle|^2 \langle\hat{A}\rangle_w^{\psi,\uparrow*} \langle\hat{B}\rangle_w^{\psi,\uparrow} \\ &\quad + |\langle\downarrow|\psi\rangle|^2 \langle\hat{A}\rangle_w^{\psi,\downarrow*} \langle\hat{B}\rangle_w^{\psi,\downarrow} \\ &\quad + (|\langle\uparrow|\psi\rangle|^2 \langle\hat{B}\rangle_w^{\psi,\uparrow*} \langle\hat{A}\rangle_w^{\psi,\uparrow} \\ &\quad + |\langle\downarrow|\psi\rangle|^2 \langle\hat{B}\rangle_w^{\psi,\downarrow*} \langle\hat{A}\rangle_w^{\psi,\downarrow}). \end{aligned} \quad (5)$$

Therefore, the expectation value of the product $\hat{A}\hat{B}$ of two arbitrary noncommuting observables can be determined by

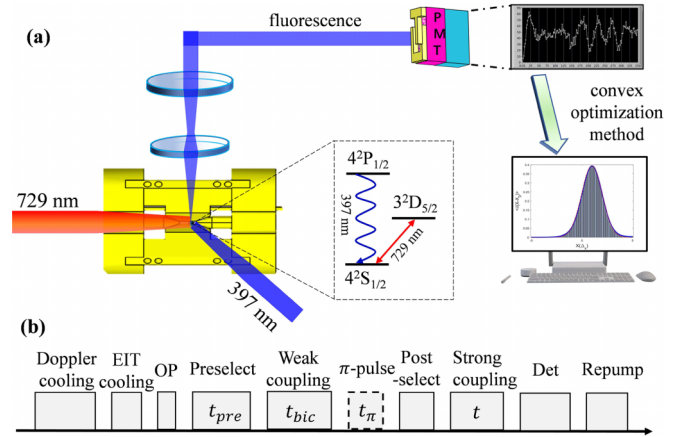


FIG. 1. (a) Illustration of the experimental setup for weak measurement with a trapped $^{40}\text{Ca}^+$ ion. The qubit states are $S_{1/2}(m_J = -1/2)$ and $D_{5/2}(m_J = -5/2)$, in our experiment, and the auxiliary state is $P_{1/2}$ used for detection. The laser at 729 nm is used to manipulate the qubits, and the laser at 397 nm is used to cool and detect. We collect fluorescence photons for state detection using the electron shelving technique. The position displacement of the motional wave packet is obtained by reconstructing the motional wave packet using convex optimization method. Panel (b) shows the sequence of the single weak measurement experiment. The solid boxes indicate the pulses that must be applied for each experiment. The dashed box indicates that if $|S\rangle$ is to be postselected, the π pulse of the carrier transition needs to be performed first.

measuring the probability $|\langle\downarrow|\psi\rangle|^2$ and the weak values of single observables \hat{A} and \hat{B} . The measurement results can be applied to verify their commutation and anticommutation relations.

III. EXPERIMENTAL SCHEME AND SETUP

The previous section introduces the theoretical measurement scheme. To verify this scheme, we need to measure the weak values of single qubit observables. According to the theoretical scheme, the weak values of the three Pauli operators postselected to $|\uparrow\rangle$ and $|\downarrow\rangle$ must be measured in the experiment. In this section, the experimental scheme and setup for measuring the weak value of Pauli operators using a single trapped $^{40}\text{Ca}^+$ ion is illustrated [31,32].

The whole setup and the main sequence of our experiment is shown in Fig. 1. We use a blade-shaped linear Paul trap with axial trapping frequency $\omega_z \approx 2\pi \times 1.33$ MHz and radial trapping frequency $\omega_r \approx 2\pi \times 1.6$ MHz to trap a single $^{40}\text{Ca}^+$ ion. The axial motion of the ion acts as the measuring pointer, and the internal electronic state of the ion is chosen as the measured system. The Zeeman sublevels $S_{1/2}(m_J = -1/2)$ and $D_{5/2}(m_J = -5/2)$ are selected as the pseudospin states $|\uparrow\rangle$ and $|\downarrow\rangle$, respectively. A narrow-linewidth laser at 729 nm, going through the two endcaps of the trap and overlapping with the axial direction of the trap, coherently couples qubit states with a Lamb-Dicke parameter of $\eta \simeq 0.08$. Using acousto-optic modulators (AOMs), the 729 nm laser can be modulated to produce the light field required for the experiment. Another important laser beam, 397 nm, which has a wave vector angle of $\pi/4$ with the 729 nm laser, is used to implement laser cooling and state detection. A photomultiplier

tube (PMT) can collect the fluorescence photons of dipole transition as the primary data. Figure 1(b) shows the sequence of weak measurement experiment. Implementing the Doppler cooling 1000 μs and EIT cooling 300 μs can prepare the motion state of the ion to the ground state. The internal electronic state of the ion can be prepared to $S_{1/2}(m_J = -1/2)$ by optical pumping (OP) for 3 μs . The preselection and weak-coupling time are set based on the experimental requirements. The postselection of 120 μs retains the data that the internal state of the ion is $|D\rangle$. The primary data were obtained by scanning the duration time t of the wave packet reconstructing operation and detecting the internal state of the ion for 300 μs .

In the trapped-ion system, the weak measurement experiment roughly consists of four steps, and we describe the experimental details of each step as follows: In a first step, the measured system should be selected to an arbitrary superposition of the eigenstates of $\hat{\sigma}_z$, which can be written as $|\psi\rangle = \cos(\theta)|\uparrow\rangle + \sin(\theta)|\downarrow\rangle$. And the measuring pointer should be prepared to the ground state, which can be described by the Gaussian wave packet $|\varphi_i(z)\rangle = (\frac{1}{2\pi\Delta_z^2})^{1/4} \exp(-\frac{z^2}{4\Delta_z^2})$, where $\Delta_z = \sqrt{\hbar/2m\omega_z}$ is the width of ground-state wave packet. Implementing Doppler cooling and electromagnetically induced transparency (EIT) cooling [33–35] using the 397 nm laser beam can prepare the external motional state of ion to the ground state. Optical pumping pulse for 3 μs can prepare the trapped ion to a pure internal state $|\uparrow\rangle$. Then a 729 nm laser beam pulse resonant with the carrier transition is applied to create an arbitrary superposition state with phase $\theta = \Omega_{\text{rot}}t_{\text{pre}}$, where $\Omega_{\text{rot}} = 2\pi \times (8.6 \pm 0.15)$ kHz is the Rabi frequency of the carrier transition. This operation has a fidelity of over 96%. At the second stage, we need to synthesize the von Neumann measurement model Hamiltonian that couple the measuring pointer and the measured system. The spin-dependent operator [36], which can be implemented by the bichromatic light field consisting of the blue and red sidebands of $|\uparrow\rangle \rightarrow |\downarrow\rangle$ transition, can help us to achieve it. This interaction Hamiltonian can be written as

$$H_{\text{bic}} = \frac{\hbar\eta\Omega_{\text{bic}}}{2}(\hat{\sigma}_x \sin\phi_+ - \hat{\sigma}_y \cos\phi_+) \otimes [(\hat{a} + \hat{a}^\dagger) \cos\phi_- + i(\hat{a}^\dagger - \hat{a}) \sin\phi_-], \quad (6)$$

where $\Omega_{\text{bic}} = 2\pi \times (19.2 \pm 0.4)$ kHz is the interaction coupling strength (less than 2 kHz drift in a month), the Pauli operators $\hat{\sigma}_x$ and $\hat{\sigma}_y$ are the qubit observables for the internal electronic state, \hat{a}^\dagger and \hat{a} are the creation and annihilation operators for the external motional state, and $\phi_+ = \frac{1}{2}(\phi_{\text{red}} + \phi_{\text{blue}})$ and $\phi_- = \frac{1}{2}(\phi_{\text{red}} - \phi_{\text{blue}})$ are the sum and the difference of the red sideband laser phase ϕ_{red} and the blue sideband laser phase ϕ_{blue} . It can be found from Eq. (6) that the measured observable is determined by setting the laser phase sum ϕ_+ and the observable of measuring pointer is determined by setting the laser phase difference ϕ_- . For example, if we set $\phi_+ = \phi_- = \frac{\pi}{2}$, Eq. (6) is changed to $H_{\text{bic}} = \eta\Omega_{\text{bic}}\Delta_z\hat{\sigma}_x\hat{p}$ with the momentum operator $\hat{p} = i(\hat{a}^\dagger - \hat{a})/2\Delta_z$. Using this Hamiltonian we can measure the weak value of observable $\hat{\sigma}_x$. Performing interaction laser pulse for a duration of t_{bic} on the initial state of the system, the total state of the system becomes

an entangled state, which can be described as

$$|\Psi\rangle = \sin\left(\theta + \frac{\pi}{4}\right)|+\rangle|\varphi_i(z + g\Delta_z)\rangle + \cos\left(\theta + \frac{\pi}{4}\right)|-\rangle|\varphi_i(z - g\Delta_z)\rangle, \quad (7)$$

where $|+\rangle = \frac{1}{\sqrt{2}}(|\uparrow\rangle + |\downarrow\rangle)$, $|-\rangle = \frac{1}{\sqrt{2}}(|\uparrow\rangle - |\downarrow\rangle)$, and weak measurement interaction coefficient $g = \eta\Omega_{\text{bic}}t_{\text{bic}}$. At this point, the external motional state wave packet of the ion is weakly displaced in two different directions. In the third step, a determined final state of the measured system is postselected by a projective measurement of the system state. We use the 397 nm laser to excite the dipole transition $|S\rangle \rightarrow |P\rangle$, then a photon is emitted due to the short lifetime of $|P\rangle$ state [37–39]. This process will destroy the external motion state of the ion when the internal state of the ion is in $|S\rangle$, in this case, the data will be discarded. The data will be reserved for the other case. This manipulation duration is 120 μs , and the detection error is measured to be less than 0.002%. However, if we want to postselect the $|S\rangle$ state, a π pulse of the carrier transition should be applied to swap the $|S\rangle$ state and $|D\rangle$ state before the projective measurement. For example, if $|\downarrow\rangle$ is selected as the postselection state and we are performing a strong projective measurement on the internal state, the external motional state wave packet changes to (the units of the position axis are Δ_z)

$$|\varphi_f(z)\rangle = \frac{1}{(2\pi)^{1/4} \sqrt{1 - \cos(2\theta)e^{-\frac{g^2}{2}}}} \times \left[\sin\left(\theta + \frac{\pi}{4}\right)e^{-\frac{(z-g)^2}{4}} - \cos\left(\theta + \frac{\pi}{4}\right)e^{-\frac{(z+g)^2}{4}} \right]. \quad (8)$$

Finally, we apply a spin-dependent operator with a strong-coupling strength $\Omega_{\text{WPR}} = 2\pi \times (96.7 \pm 9.1)$ kHz, where the observable of the measuring pointer in this step is canonically conjugated to the counterpart in the second step to reconstruct the motional wave packet [31,40] and determine its central displacement. In this step, the duration of the reconstruction pulses is varied and the fluorescence of the ion is collected the second time as the primary data. We use convex optimization method [41,42] to process the data to obtain the probability distributions of the motional wave packet in phase space. (For more details see Ref. [31].) Using Eq. (8) we can theoretically calculate the center position displacement of the external motion wave packet

$$\delta_z = \langle \varphi_f(z) | \hat{z} | \varphi_f(z) \rangle = \frac{g \sin(2\theta)}{1 - \cos(2\theta)e^{-\frac{g^2}{2}}}. \quad (9)$$

It can be found from the theory of weak measurement that the weak value can be calculated by Eq. (9) as $\langle \hat{A} \rangle_w^{\psi_f, \psi} \approx \delta_z/g$. Since the weak value is defined as a result of an approximation [21], its value is not equal to the result obtained by the practical wave-packet displacement calculation. To reduce their deviations, the value of g in the experiment is selected as small as possible. However, g also determines the probability of successful postselection, which determines the number of cycles of the experimental

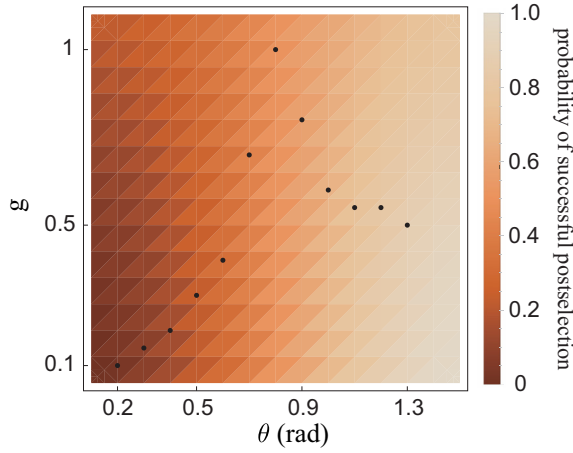


FIG. 2. The probability of successful postselection with measured observable $\hat{\sigma}_x$ and the postselected state $|\downarrow\rangle$. The color represents the size of the probability of successful postselection in different θ and g . The dark dots represent the parameters selected in the actual experiment.

sequence. The probability of successful postselection can be written as

$$P_{\text{post}} = \frac{1}{2}[1 - \cos(2\theta)e^{-\frac{g^2}{2}}]. \quad (10)$$

For instance, we set $\theta = 0.2$ rad and $g = 0.1$, the probability of successful postselection is theoretically approximately equal to 0.042. To reconstruct the external motion wave packet with high fidelity, we need to repeat the previous sequence at least 10 000 times. Hence, in order to best balance the experimental fidelity and the volume of experimental data, we simulate the postselection successful probability as a function of parameters g and θ , and we carefully choose the experimental parameters as shown in Fig. 2.

The previous four steps are only suitable for obtaining the weak value of observables $\hat{\sigma}_x$ and $\hat{\sigma}_y$. In our scheme, absolute value of the weak value of observable $\hat{\sigma}_z$ is constantly equal to 1. This is explained by the

following:

$$\langle \hat{\sigma}_z \rangle_w = \frac{\langle \uparrow | \hat{\sigma}_z | \psi \rangle}{\langle \uparrow | \psi \rangle} = \frac{\cos(\theta)}{\cos(\theta)} = -\frac{\langle \downarrow | \hat{\sigma}_z | \psi \rangle}{\langle \downarrow | \psi \rangle} = \frac{\sin(\theta)}{\sin(\theta)} = 1. \quad (11)$$

Therefore, we only need to measure the weak values of $\hat{\sigma}_x$ and $\hat{\sigma}_y$ in the experiment.

IV. EXPERIMENTAL RESULT AND DISCUSSION

To obtain the expectation value of the product of Paul operators, the weak values for single observable and the probability of the initial state $|\psi\rangle$ projected to final state $|\downarrow\rangle$ should be measured in the experiment. The experimental results for the single weak values of $\hat{\sigma}_x$ and $\hat{\sigma}_y$ are shown in Figs. 3(a) and 3(b), respectively. The probability $|\langle \uparrow | \psi \rangle|^2$ can be calculated by $|\langle \uparrow | \psi \rangle|^2 = 1 - |\langle \downarrow | \psi \rangle|^2$, where the results for $|\langle \downarrow | \psi \rangle|^2$ is shown in Fig. 3(c). To demonstrate that this scheme has no dependence on the initial state, we vary the phase θ of the initial state from 0.2 to 1.3 radians in steps of 0.1 radians. The experimental results (dots) have a remarkable agreement with the theoretical results (thick solid lines) plotted by $\langle \hat{\sigma}_x \rangle_w^{\psi, \downarrow} = \cot(\theta)$, $\langle \hat{\sigma}_x \rangle_w^{\psi, \uparrow} = \tan(\theta)$, $\langle \hat{\sigma}_y \rangle_w^{\psi, \downarrow} = i \cot(\theta)$, $\langle \hat{\sigma}_y \rangle_w^{\psi, \uparrow} = -i \tan(\theta)$, and $|\langle \psi | \downarrow \rangle|^2 = \sin^2[2](\theta)$. The weak values $\langle \hat{\sigma}_y \rangle_w$ in our scheme is a pure imaginary number. Figure 3(b) shows the imaginary part of $\langle \hat{\sigma}_y \rangle_w$. A little larger data errors at $\theta = 0.2$ radians and $\theta = 1.3$ radians points come from small postselection success probability and small motional wave packet position displacement. The long-term frequency drift of the laser at 729 nm is the main source of error in our experiments. To reduce this error, we increase the postselection success probability by adjusting the coupling strength g for weak measurements to reduce the collection time for each set of experimental data.

Using Eq. (3) and Eq. (11), the expectation value of the product of two arbitrary qubit observables and their (anti)commutation relations can be obtained. The expectation value of the operators $\hat{\sigma}_x \hat{\sigma}_y$, $\hat{\sigma}_y \hat{\sigma}_x$, $\hat{\sigma}_y \hat{\sigma}_z$, and $\hat{\sigma}_z \hat{\sigma}_y$ are shown in Figs. 4(a) and 4(c), and the experimental results agree well with the theoretical predictions $\langle \hat{\sigma}_x \hat{\sigma}_y \rangle = i \cos(2\theta)$, $\langle \hat{\sigma}_y \hat{\sigma}_x \rangle =$

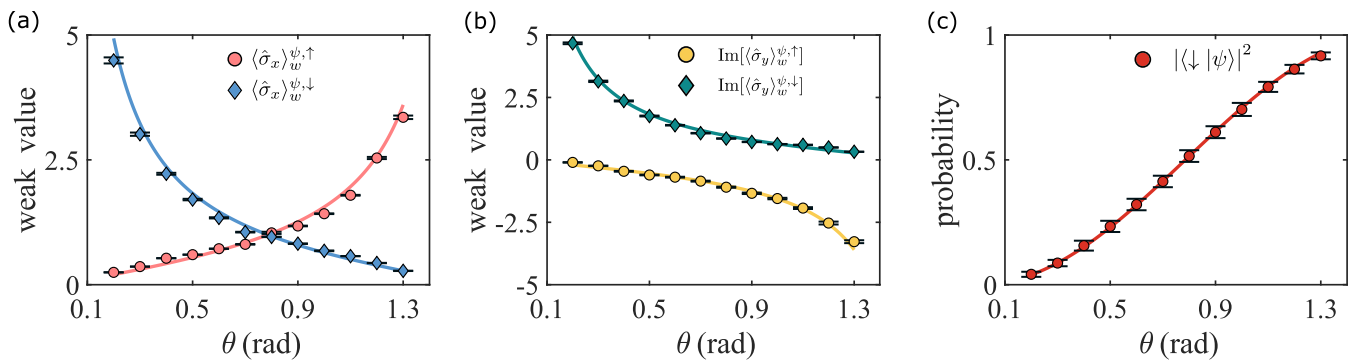


FIG. 3. The weak values $\langle \hat{\sigma}_x \rangle_w^{\psi, \downarrow(\uparrow)}$, $\langle \hat{\sigma}_y \rangle_w^{\psi, \downarrow(\uparrow)}$ measured in experimental are shown in panels (a) and (b), respectively. The experimental results of $|\langle \psi | \downarrow \rangle|^2$ are shown in panel (c). The horizontal axis is θ in the initial state $|\psi\rangle$, and the vertical axis is the weak value and the measured probability. The makers represent the experimental data, while the solid lines denote the theoretical results, the error bars of the weak values represent the size of the error in fitting the center of the motional wave packet, and the error bars of the projective probability are the standard deviation of the binomial distribution of measurements.

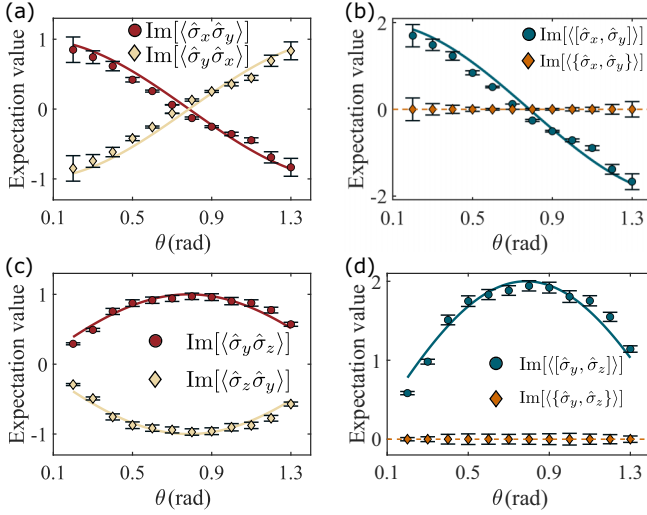


FIG. 4. Panels (a) and (c) show the imaginary part of the expectation value of operators $\hat{\sigma}_x\hat{\sigma}_y$, $\hat{\sigma}_y\hat{\sigma}_x$, $\hat{\sigma}_y\hat{\sigma}_z$, and $\hat{\sigma}_z\hat{\sigma}_y$, respectively. The symbols are the experimental results. The lines are the accurate theoretical results. Panels (b) and (d) demonstrates imaginary part of the expectation value of commutation and anticommutation relations. The symbols are the experimental data, while the solid and dotted lines are the theoretical results of commutation and anticommutation relations. The error bars are calculated using the error propagation formula based on the data in Fig. 3.

$-i\cos(2\theta)$, $\langle\hat{\sigma}_y\hat{\sigma}_z\rangle = i\sin(2\theta)$, and $\langle\hat{\sigma}_z\hat{\sigma}_y\rangle = -i\sin(2\theta)$. It can be found from the experimental results that $\langle\hat{\sigma}_x\hat{\sigma}_y\rangle$ is not equal to $\langle\hat{\sigma}_y\hat{\sigma}_x\rangle$ and is mutually complex conjugate, indicating that the operators $\hat{\sigma}_x$ and $\hat{\sigma}_y$ are noncommutative. The expectation values of the product of the two Pauli operators in our experimental results are pure imaginary numbers, which indicate that $\hat{\sigma}_x\hat{\sigma}_y$, $\hat{\sigma}_y\hat{\sigma}_x$, $\hat{\sigma}_y\hat{\sigma}_z$, and $\hat{\sigma}_z\hat{\sigma}_y$ are non-Hermitian operators. The expectation values of the (anti)commutation relation $[\hat{\sigma}_x, \hat{\sigma}_y]$ and $[\hat{\sigma}_y, \hat{\sigma}_z]$ are calculated by Eqs. (4) and (5), shown in Figs. 4(b) and 4(d), respectively. The theoretical results of the expectation value of the commutation relations, represented with the solid lines in Fig. 4, are plotted by $2i\langle\hat{\sigma}_z\rangle = 2i\cos(2\theta)$ and $2i\langle\hat{\sigma}_x\rangle = 2i\sin(2\theta)$, respectively. The expectation values of their anticommutation relations are equal to zero, indicated by the orange dashed lines. From our experimental results, the (anti)commutation relations of Pauli operators have been well verified by measuring their expectation values. To further verify the accuracy of our scheme, $\langle[\hat{\sigma}_x, \hat{\sigma}_y]\rangle$, $2i\langle\hat{\sigma}_z\rangle$, and their difference are shown in Fig. 5. The dark blue dots depict the magnitude of the difference between $\text{Im}(\langle[\hat{\sigma}_x, \hat{\sigma}_y]\rangle)$ and $2\langle\hat{\sigma}_z\rangle$. The difference is due to the accumulation of errors from each weak measurement. Selecting appropriate parameters g during theoretical design and improving the fidelity of single rotation operation can minimize these differences.

Note that the expectation value of the product of $\hat{\sigma}_x$ and $\hat{\sigma}_z$ is not shown in this work due to the fact that the initial state is the eigenstate of $\hat{\sigma}_z$, in this case the measurement for their product is transformed to be just the $\hat{\sigma}_x$. According to the commutation relation, there exists $\langle[\hat{\sigma}_x, \hat{\sigma}_z]\rangle = 2i\langle\hat{\sigma}_y\rangle$, so the (anti)commutation relations is equal to zero constantly since

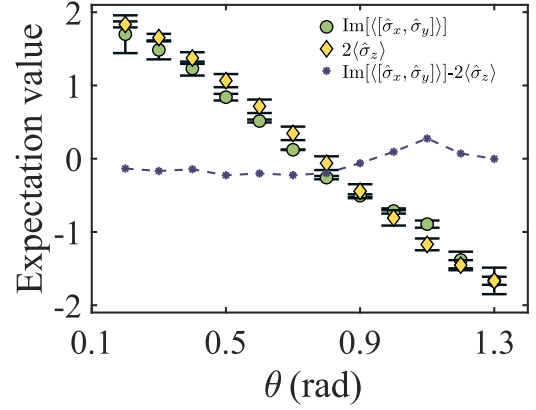


FIG. 5. The difference of $\text{Im}(\langle[\hat{\sigma}_x, \hat{\sigma}_y]\rangle)$ and $2\langle\hat{\sigma}_z\rangle$. The green balls represent the value of $\text{Im}(\langle[\hat{\sigma}_x, \hat{\sigma}_y]\rangle)$, and the yellow square blocks represent the value of $2\langle\hat{\sigma}_z\rangle$. The dark blue dotted line represents their difference.

the average for $\hat{\sigma}_y$ is always zero under the initial state $|\psi\rangle$. If one wants to verify their (anti)commutation relations, the only change would be preparing the initial measured state to $|\psi\rangle = \cos(\theta)|\uparrow\rangle + e^{i\phi}\sin(\theta)|\downarrow\rangle$ with phase ϕ . Since other experimental setups are the same, this measurement is not repeated in this paper.

V. CONCLUSION

In conclusion, we present a direct scheme to measure the expectation value of the POTNO, and this scheme is verified by measuring the expectation value of operators $\hat{\sigma}_x\hat{\sigma}_y$, $\hat{\sigma}_y\hat{\sigma}_x$, $\hat{\sigma}_y\hat{\sigma}_z$, and $\hat{\sigma}_z\hat{\sigma}_y$ in a trapped-ion system. We showed that the (anti)commutation relations of qubit observables are well agreed with the theoretical predictions with above the expectation value measurement. Since the error of multiple weak measurement experiments will eventually accumulate to the measurement result of the POTNO and the probability of successful postselection is relatively small, a large amount of measurement is required to improve the final measurement fidelity of the POTNO. Fortunately, our experimental scheme and the trapped-ion system allow easily to select a suitable initial state and coupling strength g , therefore the fidelity of the measurement and the probability of successful postselection can be balanced. The average of the product of two observables is generally defined as their correlation function, hence the measurement scheme presented in this paper would help us to study the correlation between these two observables. Using this value to verify the (anti)commutation relations is beneficial for understanding the qubit operators. Even though our scheme is only verified for measuring the expectation value of the POTNO, it is applicable to case for any number of operators. Furthermore, our scheme also can be extended to measure the average of the arbitrary non-Hermitian operator of the two-level system, since these operators can be decomposed by Pauli operators. The non-Hermitian term in the decomposition is generally represented by the product of Pauli operators, and our scheme provides a solution for measuring the average value of this term.

ACKNOWLEDGMENTS

This work is supported by the Innovation Program for Quantum Science and Technology under Grant No. 2021ZD0301601 and the National Natural Science Foundation of China under Grants No. 12004430, No. 12074433,

No. 12174447, No. 12204543, and No. 12174448. J.Z. acknowledges the support from the Science and Technology Innovation Program of Hunan Province under Grant No. 2022RC1194 and Natural Science Foundation of Hunan province under Grant No. 2023JJ10052.

- [1] W. Heisenberg, Über den anschaulichen inhalt der quantentheoretischen kinematik und mechanik, in *Original Scientific Papers Wissenschaftliche Originalarbeiten*, edited by W. Blum, H. Rechenberg, and H.-P. Dürr (Springer, Berlin, Heidelberg, 1985), pp. 478–504.
- [2] H. P. Robertson, The uncertainty principle, *Phys. Rev.* **34**, 163 (1929).
- [3] J. Erhart, S. Sponar, G. Sulyok, G. Badurek, M. Ozawa, and Y. Hasegawa, Experimental demonstration of a universally valid error–disturbance uncertainty relation in spin measurements, *Nat. Phys.* **8**, 185 (2012).
- [4] L. A. Rozema, A. Darabi, D. H. Mahler, A. Hayat, Y. Soudagar, and A. M. Steinberg, Violation of Heisenberg’s measurement-disturbance relationship by weak measurements, *Phys. Rev. Lett.* **109**, 100404 (2012).
- [5] S. Sponar, G. Sulyok, J. Erhart, and Y. Hasegawa, Error-disturbance uncertainty relations in neutron-spin measurements, *Adv. High Energy Phys.* **2014**, 735398 (2014).
- [6] G. Sulyok, S. Sponar, B. Demirel, F. Buscemi, M. J. W. Hall, M. Ozawa, and Y. Hasegawa, Experimental test of entropic noise-disturbance uncertainty relations for spin-1/2 measurements, *Phys. Rev. Lett.* **115**, 030401 (2015).
- [7] B. Demirel, S. Sponar, A. A. Abbott, C. Branciard, and Y. Hasegawa, Experimental test of an entropic measurement uncertainty relation for arbitrary qubit observables, *New J. Phys.* **21**, 013038 (2019).
- [8] Y. Hasegawa, S. Menhart, R. Meixner, and G. Badurek, Non-commutation of pauli spin operators in neutron polarimetry, *Phys. Lett. A* **234**, 322 (1997).
- [9] A. Zavatta, V. Parigi, M. S. Kim, H. Jeong, and M. Bellini, Experimental demonstration of the bosonic commutation relation via superpositions of quantum operations on thermal light fields, *Phys. Rev. Lett.* **103**, 140406 (2009).
- [10] X.-C. Yao, J. Fiurášek, H. Lu, W.-B. Gao, Y.-A. Chen, Z.-B. Chen, and J.-W. Pan, Experimental realization of programmable quantum gate array for directly probing commutation relations of Pauli operators, *Phys. Rev. Lett.* **105**, 120402 (2010).
- [11] Y.-S. Kim, H.-T. Lim, Y.-S. Ra, and Y.-H. Kim, Experimental verification of the commutation relation for Pauli spin operators using single-photon quantum interference, *Phys. Lett. A* **374**, 4393 (2010).
- [12] A. G. Wagh, V. C. Rakhecha, J. Summhammer, G. Badurek, H. Weinfurter, B. E. Allman, H. Kaiser, K. Hamacher, D. L. Jacobson, and S. A. Werner, Experimental separation of geometric and dynamical phases using neutron interferometry, *Phys. Rev. Lett.* **78**, 755 (1997).
- [13] H. Mori, A continued-fraction representation of the time-correlation functions, *Prog. Theor. Phys.* **34**, 399 (1965).
- [14] J. van Leeuwen, J. Groeneveld, and J. de Boer, New method for the calculation of the pair correlation function. I, *Physica* **25**, 792 (1959).
- [15] P. A. M. Dirac, *The Principles of Quantum Mechanics* (Oxford University Press, Clarendon, 1981).
- [16] C. M. Bender, D. C. Brody, and H. F. Jones, Complex extension of quantum mechanics, *Phys. Rev. Lett.* **89**, 270401 (2002).
- [17] C. M. Bender and S. Boettcher, Real spectra in non-Hermitian Hamiltonians having \mathcal{PT} symmetry, *Phys. Rev. Lett.* **80**, 5243 (1998).
- [18] W.-C. Wang, Y.-L. Zhou, H.-L. Zhang, J. Zhang, M.-C. Zhang, Y. Xie, C.-W. Wu, T. Chen, B.-Q. Ou, W. Wu, H. Jing, and P.-X. Chen, Observation of \mathcal{PT} -symmetric quantum coherence in a single-ion system, *Phys. Rev. A* **103**, L020201 (2021).
- [19] H. C. Baker and R. L. Singleton, Non-Hermitian quantum dynamics, *Phys. Rev. A* **42**, 10 (1990).
- [20] L. M. Johansen, Quantum theory of successive projective measurements, *Phys. Rev. A* **76**, 012119 (2007).
- [21] Y. Aharonov, D. Z. Albert, and L. Vaidman, How the result of a measurement of a component of the spin of a spin-1/2 particle can turn out to be 100, *Phys. Rev. Lett.* **60**, 1351 (1988).
- [22] A. Matzkin, Weak measurements in non-Hermitian systems, *J. Phys. A: Math. Theor.* **45**, 444023 (2012).
- [23] M. J. W. Hall, A. K. Pati, and J. Wu, Products of weak values: Uncertainty relations, complementarity, and incompatibility, *Phys. Rev. A* **93**, 052118 (2016).
- [24] M. Huang, R.-K. Lee, L. Zhang, S.-M. Fei, and J. Wu, Simulating broken \mathcal{PT} -symmetric Hamiltonian systems by weak measurement, *Phys. Rev. Lett.* **123**, 080404 (2019).
- [25] G. Nirala, S. N. Sahoo, A. K. Pati, and U. Sinha, Measuring average of non-Hermitian operator with weak value in a Mach-Zehnder interferometer, *Phys. Rev. A* **99**, 022111 (2019).
- [26] J. Lundeen and K. Resch, Practical measurement of joint weak values and their connection to the annihilation operator, *Phys. Lett. A* **334**, 337 (2005).
- [27] A. K. Pati, U. Singh, and U. Sinha, Measuring non-Hermitian operators via weak values, *Phys. Rev. A* **92**, 052120 (2015).
- [28] R. Wagner, W. Kersten, A. Danner, H. Lemmel, A. K. Pati, and S. Sponar, Direct experimental test of commutation relation via imaginary weak value, *Phys. Rev. Res.* **3**, 023243 (2021).
- [29] J. Neumann, E. P. Wigner, and R. Hofstadter, *Mathematical Foundations of Quantum Mechanics* (Princeton University Press, Princeton, NJ, 1955).
- [30] J. Dressel, M. Malik, F. M. Miatto, A. N. Jordan, and R. W. Boyd, Colloquium: Understanding quantum weak values: Basics and applications, *Rev. Mod. Phys.* **86**, 307 (2014).
- [31] C.-W. Wu, J. Zhang, Y. Xie, B.-Q. Ou, T. Chen, W. Wu, and P.-X. Chen, Scheme and experimental demonstration of fully atomic weak-value amplification, *Phys. Rev. A* **100**, 062111 (2019).
- [32] Y. Pan, J. Zhang, E. Cohen, C.-w. Wu, P.-X. Chen, and N. Davidson, Weak-to-strong transition of quantum mea-

- surement in a trapped-ion system, *Nat. Phys.* **16**, 1206 (2020).
- [33] G. Morigi, J. Eschner, and C. H. Keitel, Ground state laser cooling using electromagnetically induced transparency, *Phys. Rev. Lett.* **85**, 4458 (2000).
- [34] C. F. Roos, D. Leibfried, A. Mundt, F. Schmidt-Kaler, J. Eschner, and R. Blatt, Experimental demonstration of ground state laser cooling with electromagnetically induced transparency, *Phys. Rev. Lett.* **85**, 5547 (2000).
- [35] J. Zhang, M.-C. Zhang, Y. Xie, C.-W. Wu, B.-Q. Ou, T. Chen, W.-S. Bao, P. Haljan, W. Wu, S. Zhang, and P.-X. Chen, Parallel electromagnetically induced transparency near ground-state cooling of a trapped-ion crystal, *Phys. Rev. Appl.* **18**, 014022 (2022).
- [36] A. Sørensen and K. Mølmer, Entanglement and quantum computation with ions in thermal motion, *Phys. Rev. A* **62**, 022311 (2000).
- [37] W. Nagourney, J. Sandberg, and H. Dehmelt, Shelved optical electron amplifier: Observation of quantum jumps, *Phys. Rev. Lett.* **56**, 2797 (1986).
- [38] J. C. Bergquist, R. G. Hulet, W. M. Itano, and D. J. Wineland, Observation of quantum jumps in a single atom, *Phys. Rev. Lett.* **57**, 1699 (1986).
- [39] T. Sauter, W. Neuhauser, R. Blatt, and P. E. Toschek, Observation of quantum jumps, *Phys. Rev. Lett.* **57**, 1696 (1986).
- [40] S. Wallentowitz and W. Vogel, Reconstruction of the quantum mechanical state of a trapped ion, *Phys. Rev. Lett.* **75**, 2932 (1995).
- [41] M. Grant and S. Boyd, CVX: Matlab software for disciplined convex programming, <http://cvxr.com/cvx> (2014).
- [42] M. Grant and S. Boyd, Graph implementations for nonsmooth convex programs, in *Recent Advances in Learning and Control*, Lecture Notes in Control and Information Sciences, edited by V. Blondel, S. Boyd, and H. Kimura (Springer-Verlag Limited, London, 2008), pp. 95–110.